Inorganica Chimica Acta 547 (2023) 121360

Contents lists available at ScienceDirect

Inorganica Chimica Acta

journal homepage: www.elsevier.com/locate/ica

Electrochemical, spectroelectrochemical, and electrocatalytic properties of novel soluble phthalocyanines containing peripheral thymoxy and chloride units

Rovshen Atajanov [a,b], Berfin Huraibat [a,c], Zafer Odabaş [a,*], Ali Rıza Özkaya [a,*]

[a] Department of Chemistry, Marmara University, Faculty of Science, Kadıköy 34722, Istanbul, Turkey
[b] University of Southern Denmark, Mads Clausen Institute, SDU CAPE, 6400 Sønderborg, Denmark
[c] Bogazici University, Department of Secondary Science and Mathematics Education, Bebek 34342, Istanbul, Turkey

ARTICLE INFO

Keywords:
Phthalocyanines
Synthesis
Thymoxy
Electrochemistry
İn-situ Spectroelectrochemistry
Electrocatalitic activity

ABSTRACT

Novel CoPc, CuPc, Fe(OAc)Pc and Mn(Cl)Pc were synthesized by using original 4-chloro-5-(2-isopropyl-5-methylphenoxy)phthalonitrile in order to investigate their potential redox applications suitable with their chemical and physical characteristics. The molecular structures of new compounds were determined with spectroscopic methods such as elemental analysis, FT-IR, UV–*vis*, NMR and MALDI TOF MS. Redox behaviours of Fe(OAc)Pc and Mn(Cl)Pc complexes have been probed by using diverse voltammetric techniques such as cyclic (CV) and square wave voltammetry (SWV). In addition, the colour alterations accompanying spectral changes were perused concurrently with electrocolorimetric measurements, and electrocatalytic efficiencies of the all compounds were perused in oxygen reduction reaction.

1. Introduction

Cyclic oligopyrrole derivatives with π-conjugated structures play a significant role in natural biochemical reactions. The importance of tetrapyrrolic compounds such as heme, cytochrome, and chlorophyll in biological systems is indisputable. For instance, heme compounds are significant components of respiration, cytochromes used as redox-catalysts, and chlorophylls are responsible for photosynthesis in plants [1]. Phthalocyanines (Pcs), which consist of four isoindole rings bridged by nitrogen atoms, are synthetic analogues of porphyrins, found in nature, at the same time, they have a wider usage area than porphyrins in many applications due to their stability, structural design flexibility, and broader spectroscopic properties [2].

Because of their unique electron transfer properties, almost all of which rely on conjugated electron ring systems and the interaction of the electron system with core metal ions and peripheral and non-peripheral substituents, metallophthalocyanines (MPcs) are highly promising for especially electrocatalysis, electrochromism, and energy-producing devices such as fuel cell devices [3,4]. Therefore, it is crucial to synthesize and analyse the redox properties of newly synthesized MPcs for utilization in these technological applications [5,6]. On the other hand, some MPcs are barely soluble in common organic solvents or aqueous media. The poor solubility in Pcs also limits their use in low-cost technologies. Therefore, many explorative activities have focused on synthesizing soluble Pcs by adding functional groups to the molecule, such as poly hydroxyl, carboxyl or quaternary ammonium (for water) and bulky groups, macrocycles or long alkyl chains (for organic solvents) [7,8].

In this study, to synthesize soluble MPcs and expand their application areas, we chose thymol as a starting compound because it contains the bulky and non-bulky alkyl groups. Thus, we obtained substituted tetrachloride tetrathymoxy bearing phthalocyanine Co(II), Cu(II), Fe(III) and Mn(III) complexes, and they showed high solubility in common organic solvents (Scheme 1). After that, we investigated electrochemical, spectroelectrochemical, electrocolorimetric and electrocatalytic properties. Firstly, we implemented voltammetric and in situ spectroelectrochemical measurements for the electrochemical characterization of the complexes. We examined the redox properties of these compounds in diverse solvents such as dichloromethane (DCM) and dimethylsulfoxide (DMSO) to understand the solvent effect. The reason we performed the in situ spectroelectrochemistry measurements was to enable us to understand whether the redox processes of MPc complexes occur in the Pc ring or in the centre of the metal. While determining the redox processes of new MPcs and the effect of possible coupled processes

* Corresponding authors.
E-mail addresses: zodabas@marmara.edu.tr (Z. Odabaş), aliozkaya@marmara.edu.tr (A.R. Özkaya).

https://doi.org/10.1016/j.ica.2022.121360
Received 29 October 2022; Received in revised form 17 December 2022; Accepted 19 December 2022
Available online 22 December 2022

such as aggregation or interaction with oxygen molecules, on electron transfer processes. Another reason for performing in situ spectroelectrochemical measurements is to analyze the colour transitions that occur during the redox processes of Pc compounds. Thus, we also gained an idea about their applicability as an electrochromic material. In this article, since results similar to the literature are obtained, the voltammogram and spectroelectrochemical analyzes of Co(II), Cu(II) compounds are not presented, but the data of Fe and Mn compounds that form oxo species are presented. Secondly, we tested the electrocatalytic strengths of Pc complexes in oxygen reduction with a bipotentiostatic rotating ring disc electrode (RRDE). Since it promotes the directly producing water with low potential and low H_2O_2 production in polymer electrolyte membrane fuel cells (PEMFCs), there has been increasing research for low-cost efficient and non-noble metal-based electrocatalysts [9].

2. Experimental

In this study, the starting compound 4-chloro-5-(2-isopropyl-5-methylphenoxy)phthalonitrile was synthesized by nucleophilic aromatic substitution reaction of the thymol (2-isopropyl-5-methylphenol), and novel CoPc, CuPc, Fe(OAc)Pc and Mn(Cl)Pc were obtained by using the starting material. The used materials, equipment and Matrix-Assisted Laser Desorption/Ionization (MALDI) sample preparation are given as supplementary information.

2.1. Synthesis

*4-chloro-5-(2-isopropyl-5-methylphenoxy)phthalonitrile (**1**)*

Thymol (2-isopropyl-5-methylphenol) (1.5 g, 10 mmol) and 4,5-dichlorophthalonitrile (1.97 g, 10 mmol) were dissolved in 50 mL anhydrous dimethylformamide (DMF). After stirring for 10 min, finely ground anhydrous K_2CO_3 (2.76 g, 20 mmol) was added by stirring. The reaction mixture was stirred at room temperature for 6 days under vacuum. After the K_2CO_3 salt was filtered off, the mixture was poured into ice water and the obtained precipitate was filtered off, washed with water and dried in a vacuum at 50 °C. The crude product was purified by column chromatography with silica gel eluting with toluene.

Compound **1** is soluble in DCM, $CHCl_3$, tetrahydrofuran (THF), acetonitrile, acetone, toluene, DMF and DMSO. Yield: 2.20 g (70.96 %). Melting point: 125 °C. Anal calculated for $C_{18}H_{15}ClN_2O$: C, 69.57; H, 4.87; N, 9.01, obtained results: C, 69.61; H, 4.99; N, 8.86. IR (KBr pellet) ν_{max} /cm^{-1}: 440, 474, 530, 638, 793, 820, 868, 909, 1017, 1058, 1086, 1134, 1149, 1193, 1239, 1254, 1276, 1304, 1349, 1365, 1386, 1412, 1450, 1487, 1552, 1569, 1588, 1620, 2232, 2870, 2928, 2972, 3037, 3100. ^{1}H-NMR (500 MHz, $CDCl_3$) δ ppm 8.54 (s, 1H), 7.44 (s, 1H), 7.34 (d, J = 7.8 Hz, 1H), 7.12 (d, J = 7.8 Hz, 1H), 6.88 (s, 1H), 2.95 (m, J = 13.76, 6.9 Hz, 1H), 2.28 (s, 3H), 1.15 (d, J = 6.9 Hz, 6H).^{13}C-NMR 158.4 (1C), 150.9 (1C), 138.2 (1C), 137.2 (1C), 135.4 (1C), 129.0 (1C), 128.2 (1C), 128.0 (1C), 121.1 (1C),119.5 (1C), 115.5 (1C),114.6 (1C), 114.5 (1C), 109.1 (1C), 27.2 (1C), 23.0 (2C) 21.0 (1C).

*General procedure for the synthesis of 2,9,16,23-tetrachloro-3,10,17,24-tetrakis-(2-isopropyl-5-methylphenoxy) substituted metallo-Phthalocyanines (**2-5**)*

A mixture 0.33 mmol (0.31 g) 4-chloro-5-(2-isopropyl-5-methylphenoxy)phthalonitrile (**1**) and 0.33 mmol metal salts [0.08 g Co$(OAc)_2{\cdot}4H_2O$, 0.07 g $Cu(OAc)_2{\cdot}2H_2O$, 0.06 g $Fe(OAc)_2$ and 0.07 g $MnCl_2{\cdot}4H_2O$] transferred to a reaction tube. Then 0.20 mL of dry DMF and 0.10 mL of dry 1,8-diazabicyclo[5.4.0]undec-7-ene (DBU) were added to this reaction mixture and was heated with stirring in the sealed glass tube for 20 min under dry N_2 atmosphere at reflux temperature. The reaction mixture cooled to room temperature and was precipitated by adding acetic acid (Except FePc and MnPc). They were precipitated by adding methanol). The precipitate was filtered and washed with water and methanol respectively for 12 h in the Soxhlet apparatus. The resulting solid was purified by column chromatography (silica gel) with $CHCl_3$/MeOH (20:1). Distillative removal of the solvents yields green crystalline solid products.

The CoPc (**2**) is soluble in toluene, $CHCl_3$, DCM, THF, DMF, and DMSO. Mp > 300° C. Yield: 25.78 mg (24 %). Anal calculated for $C_{72}H_{60}Cl_4CoN_8O_4$: C, 66.42; H, 4.64; N, 8.61, obtained results: C, 66.55; H, 4.74; N, 8.51. IR (KBr pellet) ν_{max} /cm^{-1}: 495, 582, 662, 751, 812, 885, 943, 1009, 1060, 1104, 1148, 1251, 1344, 1402, 1440, 1504, 1522, 1574, 1607, 1654, 2868, 2924, 2959, 3051. UV–*vis* (DCM): λ_{max}(nm), (logε): 281 (4,971), 330 (4.462), 611 (4.532), 674 (5.003). MS (MALDI-TOF) *m/z*: calc.: 1302.06; found: 1302.02 $[M]^+$.

The CuPc (**3**) is soluble in toluene, $CHCl_3$, DCM, THF, DMF, and DMSO. Mp > 300° C. Yield: 28.01 mg (26 %). Anal calculated for $C_{72}H_{60}Cl_4CuN_8O_4$: C, 66.18; H, 4.63; N, 8.58, obtained results: C, 66.01; H, 4.79; N, 8.71. IR (KBr pellet) ν_{max} /cm^{-1}: 492, 588, 701, 745, 811, 884, 943, 1003, 1060, 1095, 1148, 1249, 1341, 1397, 1437, 1504, 1574, 1608, 2868, 2924, 2960, 3027. UV–*vis* (DCM): λ_{max}(nm), (logε): 287 (4.950), 343 (4.932), 629 (4.737), 681 (5.180). MS (MALDI-TOF) *m/z*: calc.: 1306.67; found: 1306.01 $[M]^+$.

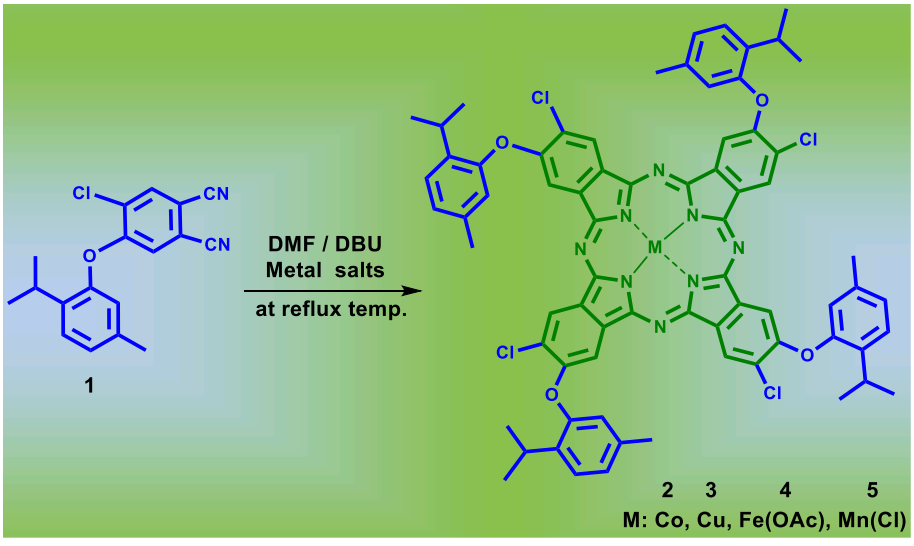

Scheme 1. Synthesis of starting material (**1**) and peripherally thymoxy (2-isopropyl-5-methylphenoxy) and chloride substituted metallo phthalocyanine (**2**–**5**) derivatives.

The Fe(OAc)*Pc* (**4**) is soluble in toluene, $CHCl_3$, DCM, THF, DMF, and DMSO. Mp > 300° C. Yield: 31.37 mg (28 %). Anal calculated for $C_{74}H_{63}Cl_4FeN_8O_6$: C, 65.45; H, 4.68; N, 8.25, obtained results: C, 65.59; H, 4.57; N, 8.11. IR (KBr pellet) ν_{max} /cm^{-1}: 502, 701, 747, 812, 885, 943, 1007, 1090, 1149, 1252, 1328, 1395, 1439, 1504, 1575, 1605, 1632, 2863, 2961, 3047. UV–*vis*(DCM): λ_{max}(nm), (logε): 281 (5.114), 362 (4.874), 670 (4.826), 711 (4.903). MS *(*MALDI-TOF*) m/z*: calc.: 1358.01; found: 1299.07 [M−OAc]$^+$.

The Mn(Cl)*Pc* (**5**) is soluble in toluene, $CHCl_3$, DCM, THF, DMF, and DMSO. Mp > 300° C. Yield: 29.70 mg (27 %). Anal calculated for $C_{72}H_{60}Cl_5MnN_8O_4$: C, 64.85; H, 4.54; N, 8.40, obtained results: C, 64.69; H, 4.69; N, 8.55. IR (KBr pellet) ν_{max} /cm^{-1}: 531, 632, 702, 743, 813, 885, 943, 1006, 1088, 1149, 1251, 1335, 1396, 1439, 1504, 1574, 1607, 2867, 2926, 2961, 3034. UV–*vis*(DCM): λ_{max}(nm), (logε): 287 (5.220), 375 (4.976), 612 (4.518), 730 (5.162). MS *(*MALDI-TOF*) m/z*: calc.: 1333.51; found: 1298.03 [M−Cl]$^+$.

2.2. Electrochemical, in - situ spectroelectrochemical, electrocolorimetric measurements

We implemented the following procedure for cyclic voltammetry (CV) and square wave voltammetry (SWV), spectroelectrochemical and electrocolorimetric measurements [6]. Super purity nitrogen gas was passed through the solutions for 20 min to remove the oxygen, and the nitrogen atmosphere was provided by keeping the inert gas above the solution during the measurement. Pt disc electrode and/or glassy carbon electrode (GCE) were used for CV and SWV measurements of all Pc compounds that were the subject of the research. These voltammetric measurements were performed separately in a super purity DMSO and DCM solvent system containing tetrabutylammonium perchlorate (TBAP) carrier electrolyte at a concentration of 0.1 M. The reference electrode (saturated calomel electrode (SCE)) and the analyte are separated by a double-layer bridge to prevent water molecules from the reference electrode inner solution from affecting the measurements. + 1.10 V to −1.85 V for CV in DMSO/TBAP medium of prepared 5x10^{-4} M concentration. While a potential of + 1.2 V − 1.9 V was applied for SWV, +1.3 V − 1.6 V for CV in DCM/TBAP environment + 1.5 V − 1.7 V for SWV was applied. In order to reduce potential control error, the reference electrode tip was positioned as close as possible to the working electrode, with the solution's uncompensated resistance a smaller fraction of the total resistance for each measurement.

For in situ UV–vis spectroelectrochemical indications with chronoamperometry, a transparent Pt gauze working electrode with a large surface area, where all redox processes can occur more clearly, was used. The measurements were carried out in a super purity DMSO and DCM solvent system containing TBAP carrier electrolyte at 0.25 M concentration. Spectral changes were recorded by applying constant potentials for certain periods in the positive and negative potential directions determined with the help of voltammograms examined consequently electrochemical measurements. In situ electrocolorimetric measurements, the colour coordinates at the beginning and end of each redox treatment were noticed.

2.3. Electrocatalytic measurements

The electrocatalytic activities of the Pc compounds in the oxygen reduction reaction (ORR) were perused by the rotating ring disk electrode (RRDE) technique by recording linear scanning voltammograms (LSV) at a rotational speed of 2500 rpm. This investigation was carried out in a 0.5 M H_2SO_4 aqueous solution medium with activated carbon (Vulcan XC-72 (VC)) containing Nafion (Nf) as support and glassy carbon working electrodes (VC/Nf/*Pc*) modified with Pc complex. The system was exposed to oxygen gas for 30 min to determine the activities of the catalysts for ORR. The modified VC/Nf/*Pc* glassy carbon ring-disc electrode used to determine the ORR performance of each catalyst consists of two working electrodes. One of the working electrodes is the Platinum ring electrode, and the other is the carbon disc electrode. While the potential of the ring electrode was polarized at 0.95 V versus the SCE, linear scanning voltammetry was applied to the disk electrode at a scanning rate of 0.005 Vs^{-1}. For each catalyst, the potential (initiation potential, E_o) and limit diffusion current density (JL), where the current starts to increase based on the value of 0.100 mA/ cm^2 were taken as the parameters determining the catalytic activity.

3. Result and discussion

3.1. Syntheses and characterization

The preparation of 4-chloro-5-(2-isopropyl-5-methylphenoxy) substituted phthalonitrile was succeed by the reaction of thymol with 4,5-dichlorophthalonitrile in dry DMF with anhydrous potassium carbonate through nucleophilic aromatic substitution reaction (Scheme 1). In the Fourier Transform Infrared (FT-IR) spectrum of the starting phthalonitrile compound **1,** the characteristic ortho di-substituted aryl chloride peaks of 4,5-dichlorophthalonitrile compound at 1734 and 1816 cm^{-1} turned into characteristic mono-substituted aryl chloride peaks at 1734, 1767, 1812 and 1836 cm^{-1} [10]. In addition, the FT-IR spectrum of the compound **1** has sharp peak appeared at 1275 cm^{-1} which corresponds aryl ether bonds (Ar−O−Ar), this result clearly indicated that 4,5-dichlorophthalonitrile was converted to the compound **1**. Strong − C≡N peak was also observed at 2234 cm^{-1} for compound **1**. This strong − C≡N peak disappeared after the formation of Pcs (**2**–**5**).

The FT-IR spectra of the Pcs were similar in most peaks, the peaks [ca. 1625 cm^{-1} (C═N str.), ca. 1606 cm^{-1} (–C═C– str.), ca. 1384 cm^{-1} (C—H bend), ca. 1275 cm^{-1} (C—O—C str.), ca. 1149 cm^{-1} (C—N str.), ca. 987 cm^{-1} (–C═C– bend)] of the Pcs were observed. The FT-IR peaks of MPcs **(2**–**5)** were almost at the same place, demonstrating that central metal had a small influence on the FT-IR vibrations.

The proton nuclear magnetic resonance (^{1}H-NMR) spectra of **1** showed characteristic signals for methyl (–CH_3) protons of isopropylgroup of thymol at δ1.15 ppm as an intense doublet peak. The methyl protons of thymol were observed at δ2.28 ppm as a singlet. The single proton of isopropyl central carbon was observed at δ 2.95 ppm as septet. The broad peak of hydroxyl (–OH) proton of thymol disappeared. Aromatic protons in the dicyanophenyl ring were observed at δ7.44 and 8.54 ppm as singlet. Aromatic proton of thymol ring at 5 position observed at δ6.88 ppm as singlet and other two aromatic protons at 3 and 4 positions of thymol ring observed at δ 7.12 and 7.34 ppm as two doublets. The molecular structure of compound **1** fully matched both the ^{1}H-NMR and ^{13}C-NMR spectra. Thus, its FT-IR and NMR spectra perfectly confirmed the molecular structure of compound **1** (Fig S1 and Fig S2).

The ion peaks of the Pcs at 1302.02([M]$^+$ for **2**), 1306.01 ([M]$^+$ for **3**), 1299.07 ([M−OAc]$^+$ for **4**) and 1298.03 Da ([M−Cl]$^+$ for **5**) were identified easily with in the reflectron mode by matrix-assisted laser desorption/ionisation time-of-flight mass (MALDI-TOF) mass spectrometry using 2,5-dihydroxybenzoic acid (DHB) as MALDI matrix. In MALDI-TOF mass spectra of all Pc compounds, peaks of (M + xH_2O) were also observed (x = 1 or 2 or.....6). This result shows that newly synthesized Pcs are highly hygroscopic compounds (Fig S3-S6).

The ultraviolet–visible (UV–*vis*) spectra of the thymol substituted Pcs exhibited a single (narrow) Q band (approximately at 674–730 nm) for compounds (**2**–**5**) as typical of MPcs with D_{4h} symmetry [11,12]. The B bands were observed at around 327–358 nm resulting from deeper π level the lowest energy unoccupied molecular orbital (LUMO) transitions. The observed sharp absorption bands are evidence for the formation of non-aggregated Pc species in various solvent (DCM, $CHCl_3$, toluene, THF, DMF and DMSO) at 5.10^{-6}M. The Q bands were observed at 674 nm for CoPc (**2**), 681 nm for CuPc (**3**), 711 nm for Fe(OAc)Pc (**4**) and 730 nm for Mn(Cl)Pc (**5**) in DCM, in Figure S7.

In addition, Mn(II)Pc, Mn(II)Pc(X)$_2$ (X coordinating solvent), (Mn

(III)Pc)$_2$O, or Mn(III)Pc kinds may observe during the synthesis, purification and electronic spectra measurements of MnPcs. The occurrences of these species also depend on the molecular structure of the Pc compounds. It generally can be predicted the existence of these species by looking to the values of Q band in the UV–*vis* spectrum. Usually, peaks in the spectrum in the range of 710–760 nm, 660–710 nm and 600–645 nm, indicate the presence of Mn(III)Pc, Mn(II)Pc, and Mn(III)Pc)$_2$O, respectively [13]. In addition, when any solution of MnPc are kept in the open air, species can transform into each other depending on solvent [12]. Similar interpretations can be made for FePc [14]. Thus, the Q band of FePc and MnPc are around 711 and 730 nm respectively, indicating that the Fe and Mn ions in the centre of this *Pc* are + 3 valances. Since Fe complex (**4**) was synthesized from Fe(OAc)$_2$ salt and Mn complex (**5**) was synthesized from $MnCl_2{\cdot}4H_2O$ salt, the axial substituents are OAc and Cl, respectively. Therefore, the molecular formulas of these complexes are shown as Fe(OAc)Pc and Mn(Cl)Pc.

3.2. Voltammetric and spectroelectrochemical characterization

We researched the electrochemical and spectroelectrochemical properties of tetra chlorine tetra thymol Fe(OAc)*Pc* and Mn(Cl)*Pc* compounds separately in DMSO and DCM solutions with TBAP. The voltammograms of the compounds examined with these techniques were recorded, and the half-peak potentials for the redox processes ($E_{1/2}$), the potential difference between the first half-peak processes ($\Delta E_{1/2}$), anodic to cathodic peak potential separations (ΔE_p), pick current ratios ($I_{pa\text{-}c}/ I_{pc\text{-}a}$) are listed in Table 1. ΔE_p values ranged 60 to 100 mV (ΔE_p of 0.080 V at 0.100 Vs^{-1} was obtained for the ferrocene internal standard) suggesting electrochemical reversible to quasi-reversible behaviour of the electron transfer processes. We found that peak currents for redox pairs of compounds are mostly directly proportional to the square root of scan rates ranging from 0.025 to 0.500 Vs^{-1}. These observations demonstrate the diffusion-controlled behaviour of redox reactions.

The voltammograms obtained regarding the redox behaviour of Compound **4** in the DCM/TBAP electrolyte system are shown in Fig. 1 (Fig. 1A: CV; Fig. 1B: SWV). Compound **4** indicates four one-electron reductions at −0,60 V, −0,90 V, −1.10 V, −1.60 V and two one-electron oxidation reactions at 0.90 V, 1.35 V. The initial oxidation and the first reduction processes of Fe(OAc)Pc were observed to occur at considerably low positive and low negative potentials. This is thanks to the energy level of the metal of the MPc having an energy level among the HOMO and LUMO of the Pc ligand, generally exhibiting both metal-based and ring-based redox processes. Fe(OAc)Pc includes a redox-active metal center, so we expect that the first redox reaction occurs on the metal center in DMSO, but the initial oxidation reaction consists on the Pc ring in DCM [15]. The data and observations in this study of **4** compound with literature data show that the redox processes.

R1: $[Fe^{3+}(OAc)Pc^{2-}]/[Fe^{2+}(OAc)Pc^{2-}]^-$,
R2: $[Fe^{2+}(OAc)Pc^{2-}]^-/ [Fe^{+}(OAc)Pc^{2-}]^{2-}$,
R3: $[Fe^{+}(OAc)Pc^{2-}]^{2-}/[Fe^{+}(OAc)Pc^{3-}]^{3-}$,
R4: $[Fe^{+}(OAc)Pc^{3-}]^{3-}/[Fe^{+}(OAc)Pc^{4-}]^{4-}$,
O1: $[Fe^{3+}(OAc)Pc^{2-}]/[Fe^{3+}(OAc)Pc^{1-}]^+$ and.
O2: $[Fe^{3+}(OAc)Pc^{-}]^+/[Fe^{3+}(OAc)Pc]^{2+}$.

So we can conclude that while the first two reduction reactions are metal-based, the other reactions are ligand-based. For all redox couples except R1, ΔEp values range usually between 60 and 90 mV at diverse scan rates. This means that electron transfer processes are electrochemical reversible. R2, R3 and R4 are fully diffusion controlled due to the appropriate respective I_{pa}/I_{pc} ratios. The chemical and electrochemical reversibility of the redox reactions of Fe(OAc)Pc are proved by SWVs with forward and reverse scans (Fig. 1B). On the other hand, the initial reduction reaction appears to be split into two pairs called R1′ and R1′′. It can be thought that this is owing to the formation of an equilibrium between species that have different coordinations. At the same time the redox processes of FePcs are much more reactive to the entity of oxygen. It may be related to the existence of μ-oxo FePc species [16]. It is thought that the splitting is not caused by aggregation thanks to the fact that not all peaks are generally broad. O2, the second oxidation process, could only be observed with a square wave, as it allowed measurement at high potential (Fig. 1B).

Table.1
The electrochemical data for **2**–**3**. All electrochemical data were given versus SCE.

Pcs	Redox Processes	Label	[a]$E_{1/2}$ (V)	[b]ΔEp (mV)	[c]Ipa/ Ipk (V)	[d]ΔE1/ 2 (V)
FePc (DCM/ TBAP)	$[Fe^{3+}Pc^{-}]^+/ [Fe^{4+}Pc^{-}]^{2+}$	O2	1.03	–	–	(0.93) (1.13)
	$[Fe^{3+}Pc^{2-}]/ [Fe^{3+}Pc^{-}]^+$	O1	0.73	65	0.98	
	$[Fe^{3+}Pc^{2-}]^+/ [Fe^{2+}Pc^{2-}]$	[e]R1′R1′′	(-0.20) (-0.40)	–	–	
	$[Fe^{2+}Pc^{2-}]/ [Fe^{+}Pc^{2-}]^-$	R2	−1.05	80	0.99	
	$[Fe^{+}Pc^{2-}]^-/ [Fe^{+}Pc^{3-}]^{2-}$	*R3*	−1.28	75	0.97	
FePc (DMSO/ TBAP)	$[Fe^{3+}Pc^{2-}]/ [Fe^{4+}Pc^{2-}]^+$	O1	0.43	100	0.9	1.08
	$[Fe^{3+}Pc^{2-}]^+/ [Fe^{2+}Pc^{2-}]$	R1	−0.65	55	1.4	
	$[Fe^{2+}Pc^{2-}]/ [Fe^{+}Pc^{2-}]^-$	R2	−1.05	75	0.95	
MnPc (DCM/ TBAP)	$[Mn^{3+}Pc^{2-}]^+/ [Mn^{3+}Pc^{-}]^{2+}$	O1	1.20	72	0.92	
	$[Mn^{3+}Pc^{2-}]^+/ [Mn^{2+}Pc^{2-}]$	R1	−0.03	60	1	1.23
	$[Mn^{2+}Pc^{2-}]/ [Mn^{+}Pc^{2-}]^-$	R2	−0.80	70	0.98	
	$[Mn^{+}Pc^{2-}]^-/ [Mn^{+}Pc^{3-}]^{2-}$	R3	−1.21	70	0.95	
	$[Mn^{+}Pc^{3-}]^{2-}/ [Mn + Pc^{4-}]^{3-}$	R4	−1.48	65	0.88	
MnPc (DMSO/ TBAP)	$[Mn^{3+}Pc^{2-}]/ [Mn^{4+}Pc^{2-}]^{2+}$	[f]O2	0.96	–	–	
	$[Mn^{4+}Pc^{2-}]^{2+}/ [Mn^{4+}Pc^{-}]^+$	O1	0.41	60	0.95	
	$[Mn^{3+}Pc^{2-}]^+/ [Mn^{2+}Pc^{2-}]$	R1	−0.04	63	1	
	$[Mn^{2+}Pc^{2-}]/ [Mn^{+}Pc^{2-}]^-$	[e]R2′ R2′′	−0.62 0.7	–	–	
	$[Mn^{+}Pc^{2-}]^-/ [Mn^{+}Pc^{3-}]^{2-}$	*R3*	−1.25	65	0.96	0.45
	$[Mn^{+}Pc^{3-}]^{2-}/ [Mn + Pc^{4-}]^{3-}$	R4	−1.68	68	1.15	

[a] : $E_{1/2} = (E_{pa} + E_{pc})/2$ at 0.10 V s^{-1}.
[b] : $\Delta E_p = E_{pa}$- E_{pc} at 0.100 V s^{-1}.
[c] : I_{pa}/I_{pc} for reduction, I_{pc}/I_{pa} for oxidation processes at 0.100 V s^{-1} scan rate.
[d] : $\Delta E_{1/2} = E_{1/2}$(first oxidation) - $E_{1/2}$ (first reduction). HOMO–LUMO gap for MPcs having an electro-inactive metal centre.
[e] : The redox behavior of the compounds was complicated by chemical reaction and thus, some redox couples were split.
[f] : These redox couples could be detected only by square wave voltammetry.

Fig. 2 shows UV–*vis* spectral alterations (Fig. 2a-2b) and obtained chromaticity diagram (Fig. 2c) of **4** in DCM/TBAP. Before applying any potential to the **4** gives the Q band around at 709 nm (red spectrum in Fig. 2a). Observation of Q band at 709 nm characterizes presence of $[Fe^{3+}(OAc)Pc^{2-}]$ species. Throughout the initial reduction reaction at −0.60 V, the Q band firstly shifts by decreasing in intensity to 632 nm (R1′) (red spectrum in Fig. 2a) and secondly shifts to 650 nm (R1′′) (blue spectrum in Fig. 8a). The absorption band at around 630 nm obviously proves that iron Pc is in the form of μ-oxo species [15]. Although the solution is decontaminated by N_2, monitoring of the band at 632 nm proves the creation of μ-oxo FePc species with the unremoved oxygen, therefore the initial reduction reaction is divided into two pairs called R1′ and R1′′. It can be thought that R1′ indicates the creation of the Pc

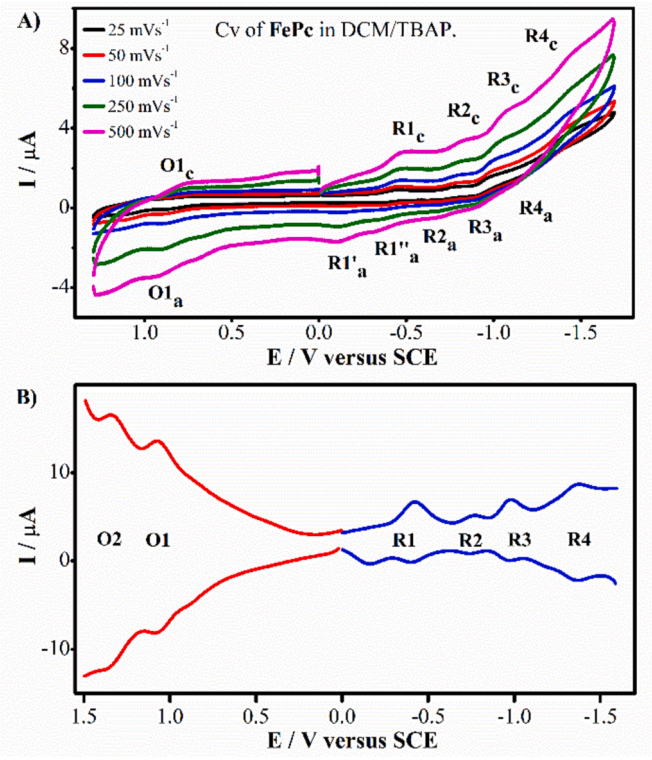

Fig. 1. (A) Cyclic and (B) square-wave voltammograms of Fe(OAc)Pc (**4**) in DCM/TBAP.

dimer anion from the μ-oxo-dimer ([$Pc^{2-}Fe^{3+}$-O-$Fe^{3+}Pc^{2-}$] ↔ [$Pc^{2-}Fe^{3+}$-O-$Fe^{2+}Pc^{2-}$]$^{-}$), and R1′′ indicates the reduction of MPc ([$Pc^{2-}Fe^{3+}$-O-$Fe^{2+}Pc^{2-}$]$^{-}$↔[$Pc^{2-}Fe^{2+}$-O-$Fe^{2+}Pc^{2-}$]$^{2-}$). The formation of ill-defined isosbestic spots during reduction supports our view that there is more than one species of reduced species. These spectral alterations by the process thanks to formation of dianionic species cause a colour alteration from green (x = 0.262, y = 0.378) to light green (x = 0.313, y = 0.394) (Fig. 2c). Throughout the second reduction reaction process at − 0.90 V (Fig. 2b). The Q band at 650 nm shift to 678 nm while a new band is recorded at 460 nm. Shifting Q band indicates the creation of [$Fe^{+}Pc^{2-}$]$^{2-}$. These changes define metal-based reduction for the R2 pair and cause a change in colour to yellow (x = 0.368, y = 0.383) (Fig. 2c).

Fig. 3 illustrates the voltammograms are available for investigating the solvent effect in DMSO/TBAP (Fig. 3A: CV; Fig. 3B: SWV). The compound **4** indicates one electron reductions at −0,80 V, −1,20 V and one electron oxidation process at 0.70 V. Redox couples were observed at −0.60 V in DCM and −0.80 V in DMSO. Since DMSO has the ability to polarize by establishing coordination, a potential shift of 0.20 V has occurred. Similarly, the first oxidation process appears to have a significantly lower potential than the DCM electrolyte system. This can be interpreted as the first oxidation of the metal-based. The literature data of Fe(OAc)Pc compound and the data and observations in this study show that the redox processes R1: [Fe^{3+}(OAc)Pc^{2-}]/[Fe^{2+}(OAc)Pc^{2-}]$^{-}$, R2:[Fe^{2+}(OAc)Pc^{2-}]$^{-}$/[Fe^{+}(OAc)Pc^{2-}]$^{2-}$,O1:[Fe^{3+}(OAc)Pc^{2-}]/[Fe^{4+}(OAc)Pc^{2-}]$^{+}$. So we can conclude that all processes are metal-based. ΔE_p value of R2 process range between 60 and 90 mV at diverse scan rates. This means that electron transfer processes are electrochemical reversible. Second reduction of **4** are fully diffusion-controlled owing to the appropriate respective Ipa/Ipc ratios. SWVs with forward and reverse scans also confirmed the chemical and electrochemical reversibility of these reactions (Fig. 3B). But the first reduction and first oxidation processes are fairly broad. It can be thought that this is thanks to the creation of an equilibrium between species that have different coordinations. Voltammetric measurement results in DMSO medium show

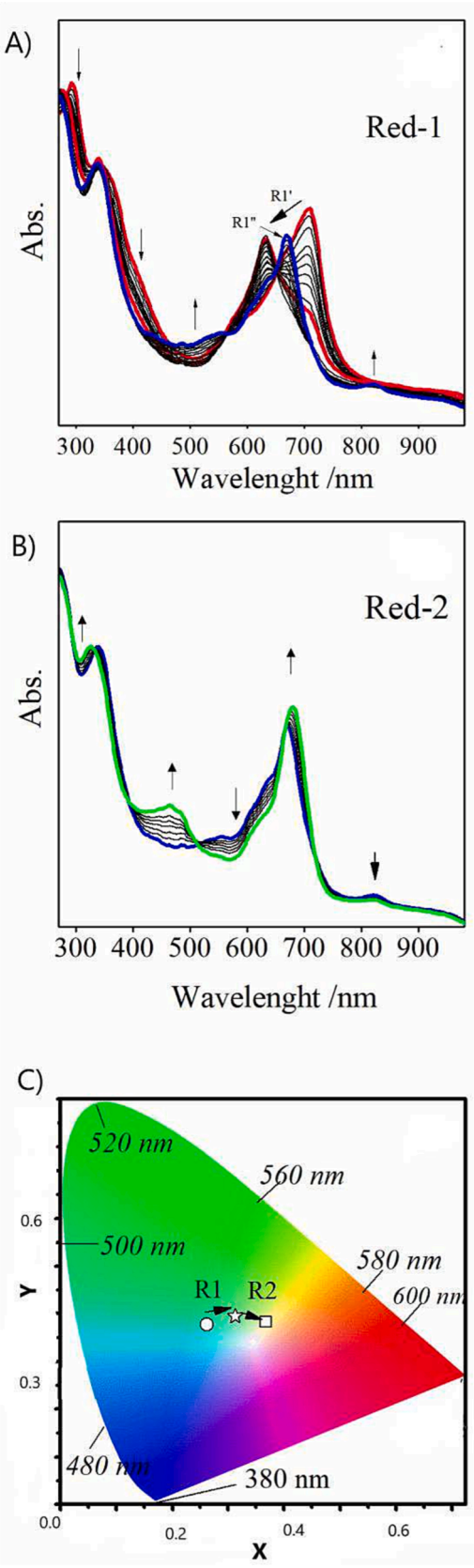

Fig. 2. In situ UV–*vis* spectral changes for (a) First reduction process (b) Second reduction process (c) Oxidation process (d) Chromaticity diagram of Fe(OAc)Pc in DCM/ TBAP.

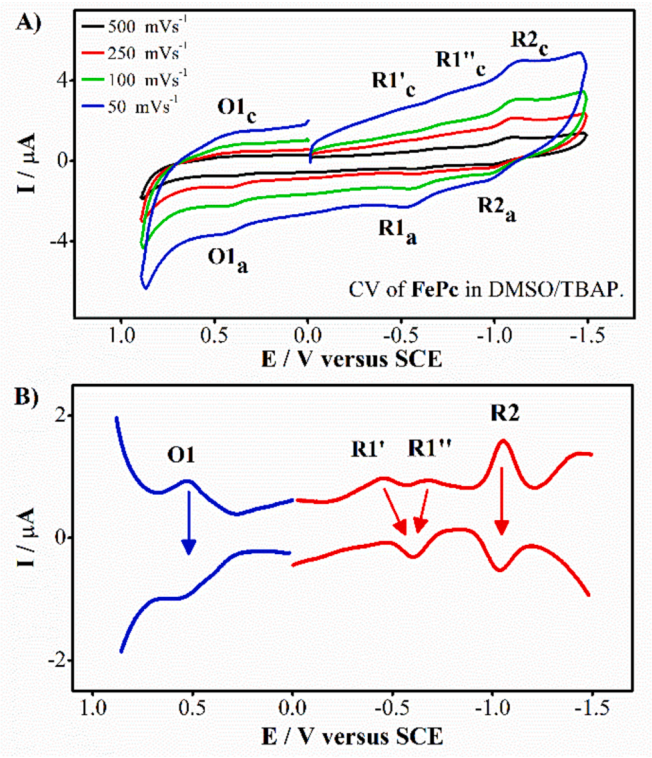

Fig. 3. (A) Cyclic and (B) square-wave voltammograms of Fe(OAc)Pc (**4**) in DMSO/TBAP.

that the solvent secures Fe(III) and therefore the compound is mostly in the form of [$OAc^{-}Fe^{3+}Pc^{2-}$]. However, the presence of differently coordinated species such as [DMSO-OAc^{-}-$Fe^{3+}Pc^{2-}$] is also expected. The first redox processes are probably complicated due to coordination tendency with the axially coordinating species in the electrolyte. Thus, the first reduction operation splits into two pairs due to equilibrium formation between the differently coordinated species, which are expected reduction at diverse potentials, and appears as a divided couple of metal-based processes.

Fig. 4 represents UV–*vis* spectral changes (Fig. 4a-4b-4c) and simultaneously obtained chromaticity diagram (Fig. 4d)) of **4** in DMSO/TBAP. Without any applied potential, **4** gives the Q band around at 630 nm (Fig. 4A). The Q band at 630 nm proves to us that iron Pc is in the form of µ-oxo species [15]. At − 0.80 V, for first reduction reaction absorption band shifts to 666 nm. The first reduction process is fairly broad. This is owing to the existence of Fe^{3+} cations with the µ-oxo-dimer structures. A shift in the band to 666 nm indicates a metal-based reduction reaction, and the existence of µ-oxo FePc species. In addition to all these, there are isosbestic points that are not clearly defined around 650 and 700 nm, and their positions have changed throughout the reduction reaction. These observations also represent that more than one species is involved in the process. In the light of this information, we can say that the spectral alterations recorded at −0.80 V are pointed out R1, [$Pc^{2-}Fe^{3+}$-O-$Fe^{3+}Pc^{2-}$] ↔ [$Pc^{2-}Fe^{2+}$-O-$Fe^{2+}Pc^{2-}$]$^{2-}$, followed by decomposition of [$Pc^{2-}Fe^{2+}$-O-$Fe^{2+}Pc^{2-}$]$^{2-}$ species to [Fe^{2+}(OAc)Pc^{2-}]$^{-}$ by the breakdown of O2 by a rapid electrochemical reaction [17,18]. These alterations cause the color differences from green (x = 0.328, y = 0.365) to light green (x = 0.352, y = 0.342) (Fig. 4d.) At −1.20 V, it is seen that the absorption band at 666 nm shifts to 683 nm and a new band is formed at 530 nm (Fig. 4b). These alterations are distinctive for metal-based reduction process also [Fe^{2+}(OAc)Pc^{2-}]$^{-}$ ↔ [Fe^{+}(OAc)Pc^{2-}]$^{2-}$ [19]. However, the band at around 630 nm still shows that the oxo species in the environment. During this transformation process, isosbestic spots also appeared at 316, 402, 585, 685 and 737 nm. Ill-defined isosbestic spots, particularly at 585 and 685 nm, define the existence of more than one reduced species. For second reduction reaction causes purple colour (x = 0.345, y = 0.275) (Fig. 4d). During this process at 0.70 V, the intensity of the 630 nm Q band decreased without shift while a new band 507 nm. These alterations illustrate oxidation of [Fe^{3+}(OAc)Pc^{2-}] to [Fe^{4+}(OAc)Pc^{2-}]$^{+}$ species. These alterations produce color differences from green to light green (x = 0.360, y = 0.399) (Fig. 4d).

The voltammograms obtained regarding the redox behaviour of Compound **5** in DCM/TBAP electrolyte system are shown in Fig. 5 (Fig. 5A: CV; Fig. 5B: SWV). Compound **5** indicates four reduction processes at −0.20 V, −1.10 V, −1.40 V, −1.60 V and one oxidation process at 1.30 V. The first reduction process of **5** was observed to occur at considerably low negative potentials similar to DCM environment. The data and observations in this study of Mn(Cl)Pc compound with literature data show that the redox processes R1:[Mn^{3+}(Cl)Pc^{2-}]$^{1+}$/[Mn^{2+}(Cl)Pc^{2-}], R2:[Mn^{2+}(Cl)Pc^{2-}]/[Mn^{+}(Cl)Pc^{2-}]$^{-}$, *R*3:[Mn^{+}(Cl)Pc^{2-}]$^{-}$/[Mn^{+}(Cl)Pc^{3-}]$^{2-}$,R4:[Mn^{+}(Cl)Pc^{3-}]$^{2-}$/[Mn^{+}(Cl)Pc^{4-}]$^{3-}$and O1:[Mn^{3+}(Cl)Pc^{2-}]$^{1+}$/[Mn^{3+}(Cl)Pc^{1-}]$^{2+}$ So we can conclude that while first two reduction reactions are metal-based, the other processes are ligand-based. For all redox couples, ΔEp values range between 60 and 90 mV at diverse scan rates. This means that electron transfer processes are electrochemical reversible. All four reduction pairs of **5** are fully diffusion controlled thanks to the appropriate respective Ipa/Ipc ratios. The chemical and electrochemical reversibility of the redox reactions of MnClPc are proved by SWVs with forward and reverse scans (Fig. 5B). During CV measurements, the anodic potentials can scan until 1.20 V in DCM/TBAP due to available potential window. The data on oxidation reaction, O1 could only be defined by SWV because during SWV measurements the anodic potentials can scan until 1.50 V in DCM/TBAP.

Fig. 6 represents UV–*vis* spectral changes (Fig. 6a-6b-6c) and simultaneously obtained chromaticity diagram (Fig. 6d)) of **5** in DCM/TBAP electrolyte system. Before applying any potential to **5**, the Q band at 731 and 522 nm proves [Mn^{3+}(Cl)Pc^{2-}] species [20](Fig. 6a). Throughout the first reduction process at −20 V, absorption band at 731 nm shifts to 682 nm, while the B band at 379 shifts to 361 nm by increasing. These alterations are defined to [Mn^{3+}(Cl)Pc^{2-}]/[Mn^{2+}(Cl)Pc^{2-}]$^{-}$ process. The shift of the absorption band to the shorter wavelength proves that the [Mn^{2+}(Cl)Pc^{2-}]$^{-}$ type has occurred [21,22]. These spectral alterations produce a colour difference from light green (x = 0.328, y = 0.365) to turquoise (x = 0.372, y = 0.380). At −1.00 V, as the intensity of the absorption band wanes, new bands are formed at 525 and 847 nm. The band at 525 nm particularly defines Mn^{+} form of the metal center of [Mn^{3+}(Cl)Pc^{2-}] [23,24]. So, we can say that this reduction reaction is [Mn^{2+}(Cl)Pc^{2-}]$^{1-}$/[Mn^{+}(Cl)Pc^{2-}]$^{2-}$(Fig. 6b). This reduction process was accompanied by the formation of a purple colour (x = 0.310, y = 0.290) (Fig. 6d). Throughout the third reduction reaction, we see that the intensity of all bands of the complex decreases (Fig. 6b inset). This observation shows us that the compound decompositions under a stationary potential of −1.40 V. Fig. 6c represents the in situ spectral alterations we observed throughout the initial oxidation reaction. The clear absorption band at 731 nm decrease without shift, and a new peak at 833 nm forms. The alterations seen throughout this oxidation reaction indicate a ring-based oxidation process, [Mn^{3+}(Cl)Pc^{2-}]/[Mn^{3+}(Cl)Pc^{-}]$^{+}$, in a non-coordinating DCM electrolyte system. These spectral changes cause a colour difference to pink (x = 0.372, y = 0.324) (Fig. 6d).

Fig. 7 illustrates the voltammogram and the square wave voltammogram are available for investigating the solvent effect in DMSO/TBAP. The compound **5** indicates four one-electron reductions at −0.30 V, −1.05 V, −1.50 V and −1.85 V and two one-electron oxidation processes at 0.41 V and 1.05 V. Reduction couples were observed at −0.20 V in DCM and −0.30 V in DMSO medium. Since DMSO has the ability to polarize by establishing coordination, a potential shift of 0.10 V has occurred. Similarly, oxidation couples were observed at 1.30 V in DCM and at 0.41 V in DMSO. This can be interpreted as the first oxidation of the metal-based. The literature data of Mn(Cl)Pc compound and the data

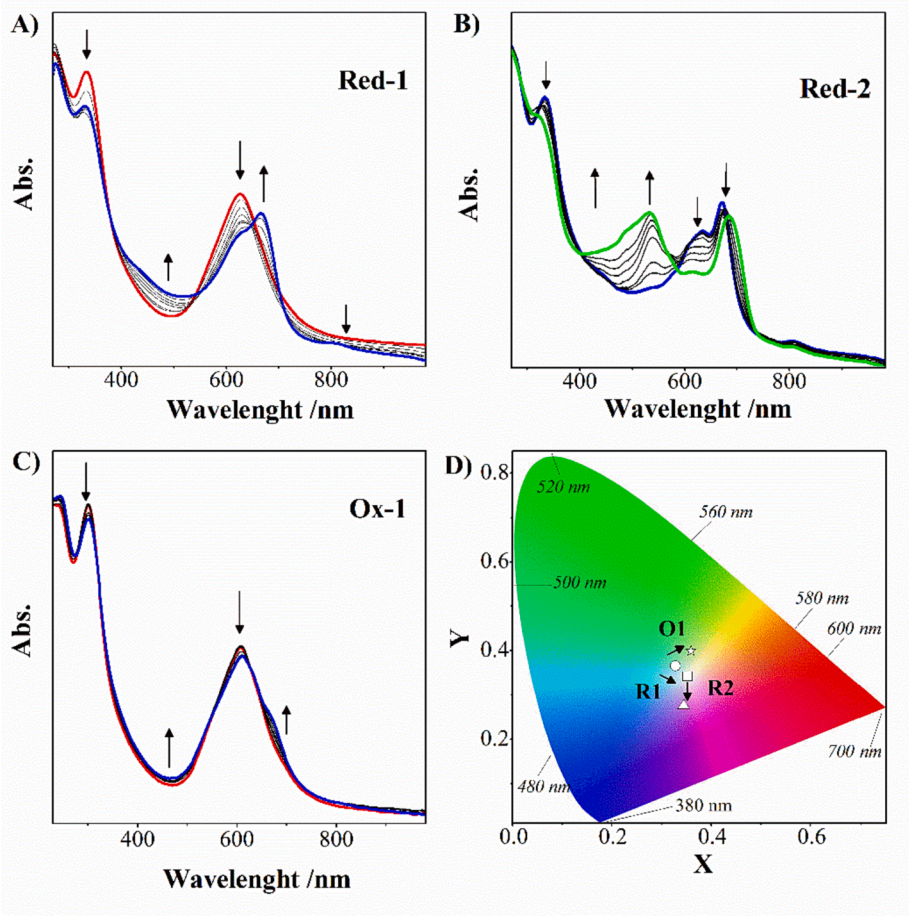

Fig. 4. In situ UV–*vis* spectral changes for (a) First reduction process (b) Second reduction process (c) Oxidation process (d) Chromaticity diagram of Mn(Cl)Pc in DMSO/ TBAP.

and observations in this examination show that the redox processes R1: $[Mn^{3+}(Cl)Pc^{2-}]/[Mn^{2+}(Cl)Pc^{2-}]^{-}$, R2:$[Mn^{2+}(Cl)Pc^{2-}]^{-}/[Mn^{+}(Cl)Pc^{2-}]^{2-}$, *R*3:$[Mn^{+}(Cl)Pc^{2-}]^{2-}/[Mn^{+}(Cl)Pc^{3-}]^{3-}$, R4:$[Mn^{+}(Cl)Pc^{3-}]^{3-}/[Mn^{+}(Cl)Pc^{4-}]^{4-}$,O1:$[Mn^{3+}(Cl)Pc^{2-}]/[Mn^{4+}(Cl)Pc^{2-}]^{+}$veO2:$[Mn^{4+}(Cl)Pc^{2-}]^{-}/[Mn^{4+}(Cl)Pc^{-}]^{2+}$. So we can conclude that initial and further reductions and initial oxidation reactions are metal-based, the other processes are ligand-based. For all redox couples except R2, ΔE_p values range usually between 60 and 90 mV at different scan rates. This means that electron transfer processes are electrochemical reversible. Except for R2 of Mn(Cl)Pc, all reduction pairs are fully diffusion controlled due to the appropriate respective Ipa/Ipc ratios. All reduction couples except R2 of Mn(Cl)Pc are fully diffusion controlled with the union of the respective Ipa/Ipc ratios. The chemical and electrochemical reversibility of the redox processes of MnClPc are proved by SWVs with forward and reverse scans (Fig. 7B). But the R2 process is divided into two pairs called R2′ and R2′′, possibly owing to the formation of equilibrium between the differently coordinated species. The second redox reaction is probably complicated due to coordination tendency with the axially coordinating species in the electrolyte. Thus, the first reduction process is divided into two pairs owing to the creation of equilibrium among the differently coordinated species. At different potentials, reduction reactions are expected and therefore appear as a divided pair of metal-based processes. At the same time the redox processes of MnPcs are much more reactive to the entity of oxygen. It might be related to the existence of μ-oxo MnPc species [16]. The data on the second oxidation reaction, O2 could only be defined by SWV because during SWV measurements the anodic potentials could scan until 1.1 V in DCM/TBAP (Fig. 7B).

Fig. 8 illustrates the UV–*vis* spectral and in situ electrocolorimetric changes of Mn(Cl)Pc are available for investigating the solvent effect in DMSO/TBAP. Before applying any potential to **5**, observation of a Q band around at 725 nm and the band at 502 nm prove $[Mn^{3+}(Cl)Pc^{2-}]$ species [25]. Also, spectrum showed very distinct peak at 631 nm with a small peak at 682 nm. The observation of a peak at 631 nm evidences the existence of MnPc μ-oxo complexes [13], while the peak at 682 nm verifies the presence of $[Mn^{2+}(Cl)Pc^{2-}]^{-}$ species. These species were observed in DMSO but not in DCM (Fig. 6a-8a). The band observed at 631 nm indicates that oxygen could not be removed even though nitrogen gas was passed through the medium. Throughout the reduction reaction, it is seen that the band at 725 nm shifts to 682 nm and the band at 502 gradually disappears. These spectral alterations are described to $[Mn^{3+}(Cl)Pc^{2-}]/ [Mn^{2+}(Cl)Pc^{2-}]^{-}$ reaction. During this transformation process, ill-defined isosbestic spots define the existence of more than one reduced species. An increase in intensity of the band at 631 nm ratified the existence of the μ-oxo with $[Mn^{3+}(Cl)Pc^{2-}]$ and the electro-generated $[Mn^{2+}(Cl)Pc^{2-}]^{-}$ species [26]. These transformations create a colour alteration from turquoise (x = 0,276, y = 0,294) to blue (x = 0,324, y = 0,352) (Fig. 8d). The second reduction reaction of **5** is also a metal-based reduction reaction, which could be appointed to $[Mn^{2+}(Cl)Pc^{2-}]^{-}/[Mn^{+}(Cl)Pc^{2-}]^{2-}$ process (Fig. 8b). Throughout the second reduction reaction, while the band at 725 nm wanes in intensity, the band at 502 nm gradually disappears. These alterations describe to $[Mn^{2+}(Cl)Pc^{2-}]^{-}$ species formation from μ-oxo species. Moreover, new bands are seen at 532, 565, 807 and 861 nm. It is determined that the intensity of the band at 682 nm increased and a new band is formed at 861 nm. While these processes confirm the $[Mn^{2+}(Cl)Pc^{2-}]^{-}$ species formation, we can confirm the presence of both $[Mn^{2+}(Cl)Pc^{2-}]^{-}$ and $[Mn^{+}(Cl)Pc^{2-}]^{2-}$ in the medium since the creation of new bands at 532 and 807 nm especially

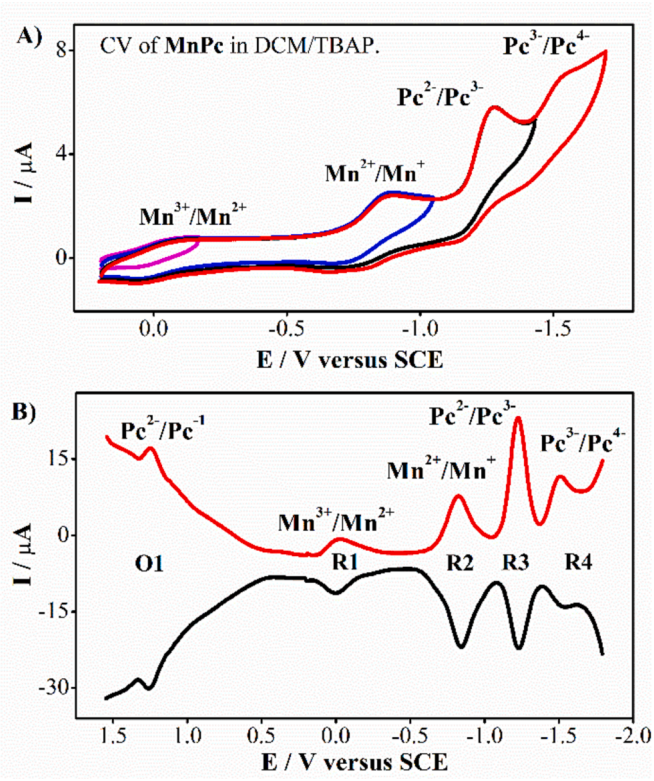

Fig. 5. (A) Cyclic and (B) square-wave voltammograms of Mn(Cl)Pc (**5**) in DCM/TBAP.

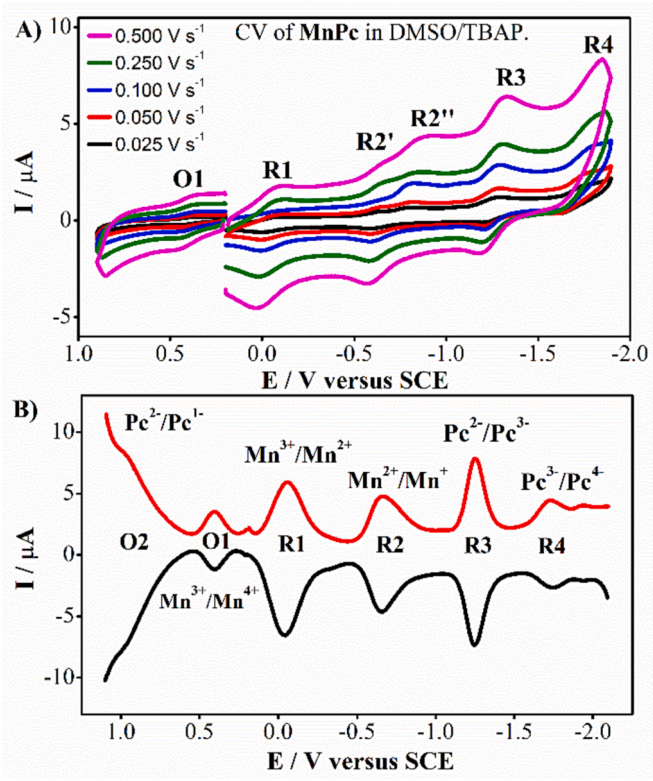

Fig. 7. (A) Cyclic and (B) square-wave voltammograms of Mn(Cl)Pc (**5**) in DMSO/TBAP.

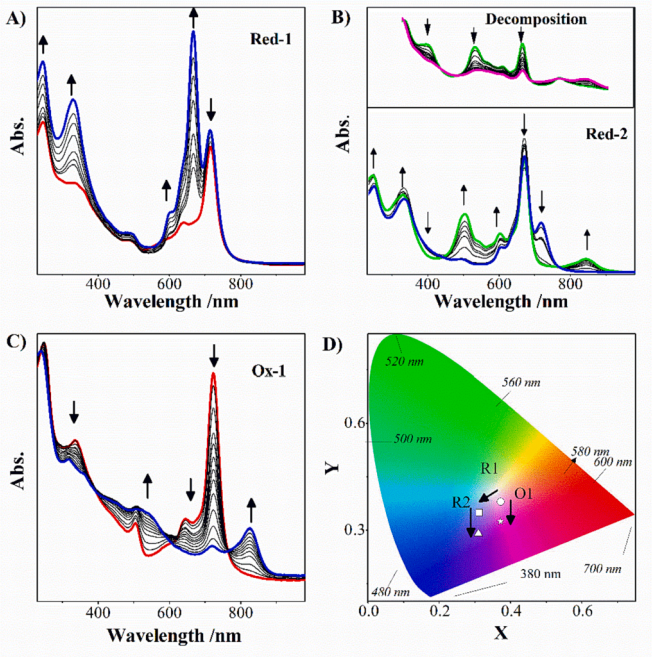

Fig. 6. In situ UV–*vis* spectral changes for (a) First reduction process (b) Second reduction process (c) Oxidation process (d) Chromaticity diagram of Mn(Cl)Pc in DCM/ TBAP.

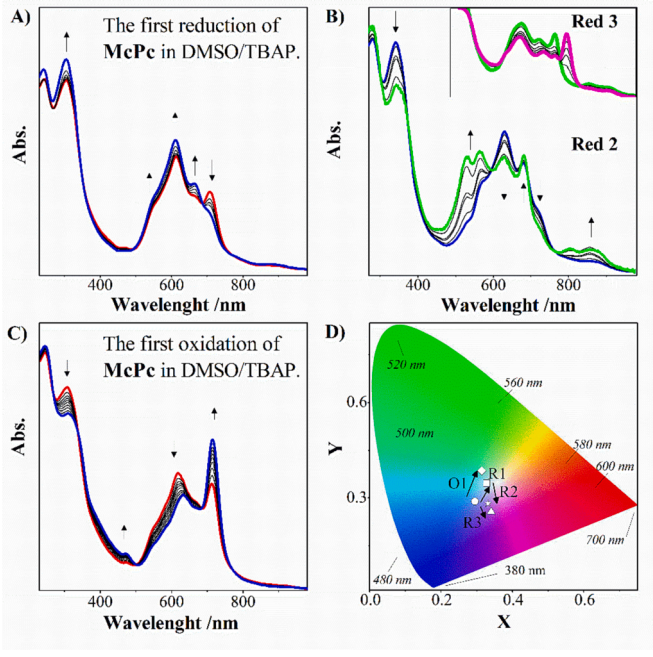

Fig. 8. In situ UV–*vis* spectral changes for (a) First reduction process (b) Second reduction process (c) Oxidation process (d) Chromaticity diagram of Mn(Cl)Pc in DMSO/ TBAP.

characterises the Mn(I) form. Not well-defined isosbestic points in the spectra also describe the existence of more than one type of reduced species. These transformations create a purple colour (x = 0.320, y = 0.301) (Fig. 8d). Fig. 8b inset shows third reduction under −1.50 V. Throughout this reduction reaction, while the bands at 410 between 470 nm boost, the bands at 620 and 690 nm wane in intensity, and a new band forms at 710 nm. These alterations indicate that the reduction reaction is taking place in the Pc-ring ($[Mn^{+}(Cl)Pc^{2-}]^{2-} \leftrightarrow [Mn^{+}(Cl)Pc^{3-}]^{3-}$)[27]. These transformations create a colour alteration from

purple to pink (x = 0,328, y = 0,262) (Fig. 8d). Fig. 8c represents in situ spectral alterations throughout the initial oxidation reaction under 0.50 V. We can see that the Q band at 725 nm increases and μ-oxo peak at 631 nm wanes. These changes describe from μ-oxo species to [Mn(III)(Cl)Pc (-2)] in coordinating DMSO electrolyte system. These transformations create a colour alteration from turquoise to green (x = 0.315, y = 0.383) (Fig. 8d).

3.3. Electrocatalytic studies for ORR

Electrocatalytic activities of 2–5 toward ORR have been studied by the ring and disk polarisation curves of a catalyst coated RRDE. The catalyst ink of the complexes was prepared by mixing each complex with VC and Nf. The catalytic activity of each complex toward ORR is shown in Fig. 9A by the relevant polarisation curve. The initial potential (E_o) where the current starts to rise and the limiting diffusion current density (J_L) were taken as criteria in the catalytic activity studies.

Table 2 sums up electrocatalytic capacities of Pc-based catalysts **2**–**5**, and compares their catalytic activities. For each catalyst, the potential (onset potential, Eo) and limit diffusion current density (JL) where the current starts to increase based on the value of 0.100 mA/cm^2 were taken as the parameters determining the catalytic activity. Results of the electrocatalytic measurements show that CoPc, **2**, Mn(Cl)Pc, **5** and Fe (OAc)Pc, **4** catalysts display remarkable catalytic performance in comparison with the CuPc, **3**. The current density reaches a plateau at J_L values of 4.27 for **2**, 0.93 for **3**, 2,46 for **4** and 1.40 mA cm^{-2} for 5 at 2500 rpm. The distinctive catalytic activity of **2**, **4**, and **5** can be connected to their redox active metal centre advancing the interaction with oxygen molecules owing to the partial electron transmission from the filled d orbitals of the metal to the empty or partially filled p * orbitals of oxygen. It is openly observed that catalytic efficiency of Fe(OAc)Pc, **4** towards ORR is much better as compared to the others. This difference can be connected to its capacity to keep dioxygen because of its marked coordinating properties, which was also reflected by high tendency to form μ-oxo [Pc^{-2}Fe^{3+}-O-Fe^{3+}Pc^{-2}] species during CV, SWV and in situ spectroelectrochemistry measurements.

Table 2
Electrocatalytic performances of **2**–**5** for ORR.

Pcs	$E_o^a$for ORR (V) vs SCE	J_L^b for ORR (mA cm^{-2})
2	+0.084	4.27
3	−0.381	0.93
4	+0.312	2.46
5	−0.176	1.40

ORR can take two different paths while producing water. It either produces water in a single step with a four-electron mechanism or completes the process by producing hydrogen peroxide through a two-step mechanism [28]. While it is desirable to have a complete reduction directly to water following the first process, in this instance a weak catalytic activity the second process takes place. For this reason, it is very important to find out the number of electrons accompanying the

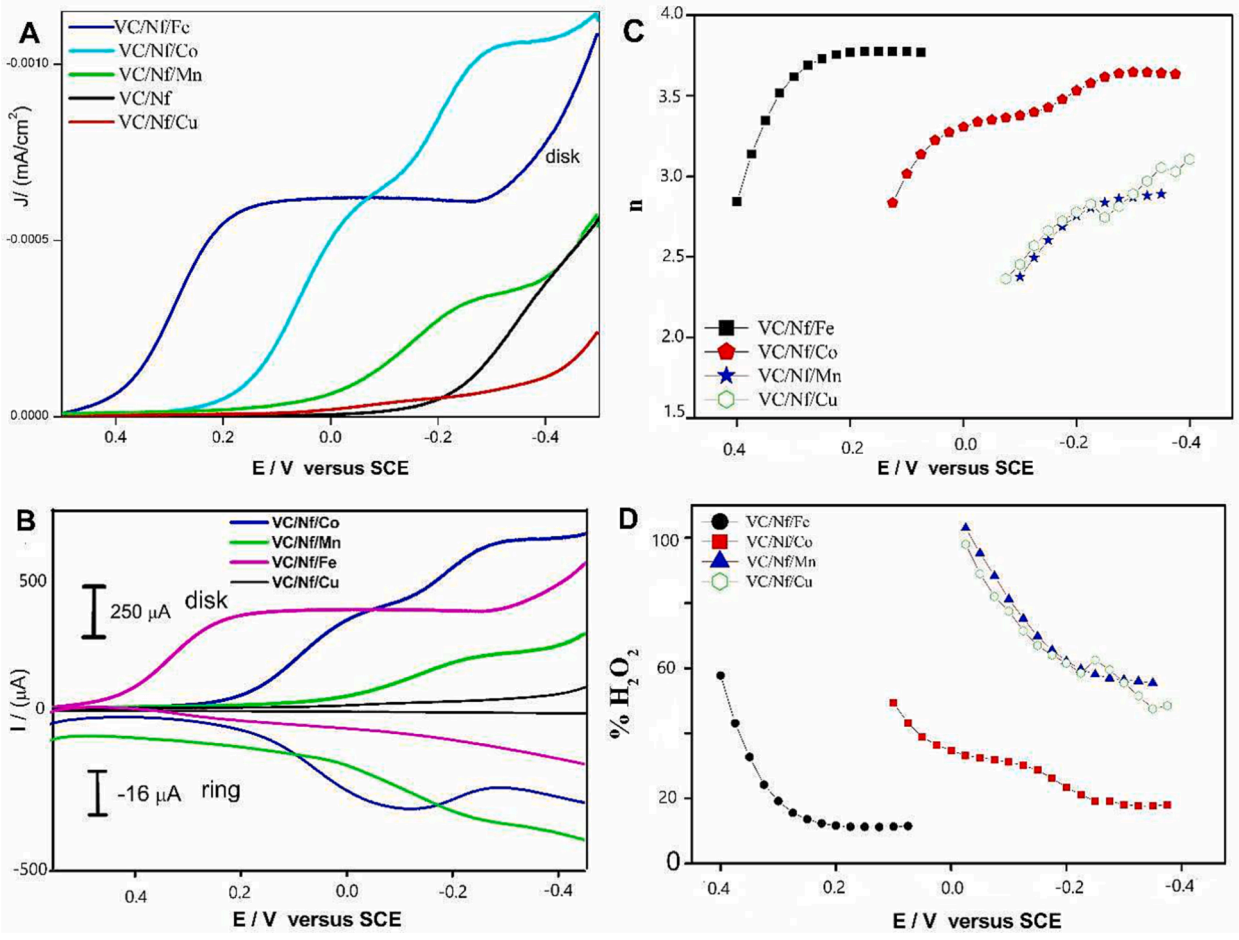

Fig. 9. (A) RDE polarization curves recorded with VC/Nf/MPc modified glassy carbon electrodes in 0.5 M H_2SO_4 solution saturated with O_2 for electrocatalytic ORR. (B) RRDE polarization curves recorded with VC/Nf/MPc modified rotating (2500 rpm) glassy carbon disc and platinum ring electrodes in 0.5 M H_2SO_4 solution saturated with O_2 for electrocatalytic ORR. (C) Variation of the total number of electrons transferred with disk potential for VC/Nf/MPc modified electrodes. (D) Variation of % H_2O_2 amount with disc potential for VC/Nf/MPc modified electrodes.

process and the amount of hydrogen peroxide in the reaction. To determine this process, RRDE measurements were made with a VC/Nf/Pc modified glassy carbon disc electrode and a polarised platinum ring electrode (Fig. 9B). Ring currents were measured to forecast the amount of hydrogen peroxide produced and the percentage of direct water generation. The number of transferred electrons nt and the resulting % H_2O_2 values were determined following equations:[28,29]

$$n_t = 4I_D/\left[I_D + \left(\frac{I_R}{N}\right)\right]$$

$$\%H_2O_2 = 100(4 - n_t)/2$$

N is collection efficiency, I_D is disk current, and I_R is ring current. Fig. 9C and Fig. 9D represent the nt and percentage of hydrogen peroxide generated as a function of potential. Among the Pcs, the best catalytic capacity was produced by the **4**-based electrode. The total number of electrons transferred in this catalyst is more significant than 2.8 at all potentials, indicating that more water is formed than H_2O_2. The nt value increases with the potential increase and takes the value of 3.76 (94 % H_2O and 6 % H_2O_2), with the main product being water, in the diffusion current plateau. The wane in the quantity of hydrogen peroxide with the potential increase in the high overvoltage area must be owing to the catalytic reduction of hydrogen peroxide to water.

4. Conclusion

In this study, the controlled nucleophilic substitution was achieved between thymol, which is high biological active materials, and 4,5-dichlorophthalonitrile compounds by using mole fraction 1/1. 4-chloro-5-(thymoxy)phthalonitrile was obtained from this reaction, and then novel excellently soluble metallo-phthalocyanines(CoPc **2**, CuPc **3**, Fe(OAc)Pc **4** and Mn(Cl)Pc **5**) containing peripheral tetra thymoxy and tetra chloride units. The electrochemical and spectroelectrochemical studies indicate that Mn(Cl)Pc and Fe(OAc)Pc complexes demonstrate metal and ligand-based one-electron redox reactions. Electrochemical and colorimetry studies, supported by in situ spectroelectrochemical measurements of the complexes, revealed that the compounds showed significant redox and electrochromic properties. Electrocatalytic efficiencies of the compounds toward ORR were examined based on the idea that the subsequent multielectron redox behaviours and coordination capability by the dioxygen molecule of those compounds may be an indicator of their possible electrocatalytic capacity. Complex Fe(Cl)Pc 4 based catalyst showed remarkable catalytic performance toward ORR. This prominent catalytic performance of **4** was referred to rich redox-active behaviour of the metal centre. In this case, it is seen that the interaction between the metal centre and the oxygen molecules increases as a result of the partial electron transfer from the occupied d orbitals of the metal to the vacant or partially filled π * orbitals.

CRediT authorship contribution statement

Rovshen Atajanov: Conceptualization, Investigation, Writing – original draft. **Berfin Huraibat:** Conceptualization, Investigation, Writing – original draft. **Zafer Odabaş:** Validation, Writing – review & editing, Supervision. **Ali Rıza Özkaya:** Validation, Writing – review & editing, Supervision.

Declaration of Competing Interest

The authors declare that they have no known competing financial interests or personal relationships that could have appeared to influence the work reported in this paper.

Data availability

Data will be made available on request.

Acknowledgments

The authors thank The Scientific Research Projects Committees of Marmara University (Project No: FEN-C-YLP-200318-0411 and FEN-C-YLP-120418-0164) for their financial support. A.R. Özkaya also thanks Turkish Academy of Sciences, TUBA for support.

Appendix A. Supplementary data

Supplementary data to this article can be found online at https://doi.org/10.1016/j.ica.2022.121360.

References

[1] D. WÖHrle, G. Schnurpfeil, 110 - Porphyrins and Phthalocyanines in Macromolecules, in: K.M. Kadish, K.M. Smith, R. Guilard (Eds.), The Porphyrin Handbook, Academic Press, Amsterdam, 2003, pp. 177–246.
[2] C.G. Claessens, W.J. Blau, M. Cook, M. Hanack, R.J. Nolte, T. Torres, D. WoËhrle, Monatshefte für Chemie/Chemical Monthly 132 (2001) 3–11.
[3] C.C. Leznoff, A.B.P. Lever, Phthalocyanines : properties and applications by edited C.C. Leznoff and A.B.P. Lever, VCH, New York, N.Y, 1993.
[4] K. Sakamoto, E. Ohno, Dyes and pigments 37 (1998) 291–306.
[5] E.T. Saka, Z. Bıyıklıoğlu, Journal of Organometallic Chemistry 745 (2013) 50–56.
[6] A.B. Sorokin, Chemical reviews 113 (2013) 8152–8191.
[7] K. Ukei, Acta Crystallographica Section B: Structural Crystallography and Crystal, Chemistry 29 (1973) 2290–2292.
[8] P. Stuzhin, O. Khelevina, B. Berezin, (1996).
[9] N. Koçyiğit, Ü.E. Özen, M. Özer, B. Salih, A.R. Özkaya, Ö. Bekaroğlu, Electrochimica Acta 233 (2017) 237–248.
[10] B.C. Pein, N.-H. Seong, D.D. Dlott, The Journal of Physical Chemistry A 114 (2010) 10500–10507.
[11] M. Sumimoto, T. Honda, Y. Kawashima, K. Hori, H. Fujimoto, Dalton Transactions 41 (2012) 7141–7150.
[12] J. Sforzini, F. Bocquet, F. Tautz, Physical Review B 96 (2017), 165410.
[13] J. Janczak, R. Kubiak, M. Śledź, H. Borrmann, Y. Grin, Polyhedron 22 (2003) 2689–2697.
[14] S. Altun, E.B. Orman, Z. Odabaş, A. Altındal, A.R. Özkaya, Dalton Transactions 44 (2015) 4341–4354.
[15] M. Stillman, T. Nyokong, C. Leznoff, A. Lever, Phthalocyanines: properties and applications, in: C.L.a.A. Lever (Ed.), VCH, New York, 1989, pp. 133.
[16] E.B. Orman, Z. Odabaş, A.R. Özkaya, Journal of The Electrochemical Society 165 (2018) H530.
[17] C. Ercolani, M. Gardini, F. Monacelli, G. Pennesi, G. Rossi, Inorganic Chemistry 22 (1983) 2584–2589.
[18] C. Ercolani, G. Rossi, F. Monacelli 44 (1980) 215–216.
[19] D. Arıcan, M. Arıcı, A.L. Uğur, A. Erdoğmuş, A. Koca, Electrochimica Acta 106 (2013) 541–555.
[20] G. Pomarico, S. Nardis, M.L. Naitana, M.G.A.H. Vicente, K.M. Kadish, P. Chen, L. Prodi, D. Genovese, R. Paolesse, Inorganic Chemistry 52 (2013) 4061–4070.
[21] Y.B. Shim, C.S. Jin, Z.Q. Feng, K. Niki, Electroanalysis 8 (1996) 1023–1028.
[22] S. Arslan, I. Yilmaz, Inorganic Chemistry Communications 10 (2007) 385–388.
[23] M. Kandaz, A. Koca, Polyhedron 28 (2009) 2933–2942.
[24] Y. Liu, X. Lin, Chinese Journal Of Analytical Chemistry 27 (1999) 1026–1028.
[25] A.L. Uğur, A. Erdoğmuş, A. Koca, U. Avcıata, Polyhedron 29 (2010) 3310–3317.
[26] M. Arıcı, D. Arıcan, A.L. Uğur, A. Erdoğmuş, A. Koca, Electrochimica Acta 87 (2013) 554–566.
[27] M. Sevim, M.N. Yaraşir, A. Koca, M. Kandaz, Dyes and Pigments 111 (2014) 190–201.
[28] S. Baranton, C. Coutanceau, E. Garnier, J.-M. Léger, Journal of Electroanalytical Chemistry 590 (2006) 100–110.
[29] M. Lefevre, J.-P. Dodelet, Electrochimica Acta 48 (2003) 2749–2760.